coatings

MDPI

Article

Surface Modification of 316L SS Implants by Applying Bioglass/Gelatin/Polycaprolactone Composite Coatings for Biomedical Applications

Behzad Mojarad Shafiee [1], Reza Torkaman [2], Mohammad Mahmoudi [2], Rahmatollah Emadi [2], Maryam Derakhshan [3], Ebrahim Karamian [1] and Fariborz Tavangarian [4,*]

1 Advanced Materials Research Center, Department of Materials Engineering, Najafabad Branch, Islamic Azad University, Isfahan 85141, Iran; behzadshafee@yahoo.com (B.M.S.); ekaramian@pmt.iaun.ac.ir (E.K.)
2 Department of Materials Engineering, Isfahan University of Technology, Isfahan 84156, Iran; rezatorkaman18@yahoo.com (R.T.); Mohammad.Mahmoudi19.9.92@gmail.com (M.M.); remadi@cc.iut.ac.ir (R.E.)
3 Department of Pathology, Al-Zahra Hospital, Isfahan University of Medical Sciences, Isfahan 81746, Iran; m_derakhshan58@yahoo.com
4 Mechanical Engineering Program, School of Science, Engineering and Technology, Pennsylvania State University, Harrisburg, Middletown, PA 17057, USA
* Correspondence: f_tavangarian@yahoo.com or fut16@psu.edu; Tel.: +1-717-948-6125

Received: 12 November 2020; Accepted: 10 December 2020; Published: 14 December 2020

Abstract: In this study, various composites of bioglass/gelatin/polycaprolactone (BG/GE/PCL) were produced and coated on the surface of 316L stainless steel (SS) to improve its bioactivity. X-ray diffractometry (XRD), scanning electron microscopy (SEM) and energy-dispersive X-ray spectroscopy (EDS) were utilized to characterize the specimens. The results showed that bioglass particles were distributed uniformly in the coating. By increasing the wt.% of bioglass in the nanocomposite coatings, the surface roughness and adhesion strength increased. The corrosion behavior of GE/PCL (PCL-10 wt.% gelatin coated on 316L SS) and 3BG/GE/PCL (GE/PCL including 3 wt.% bioglass coated on 316L SS) samples were studied in PBS solution. The results demonstrated that 3BG/GE/PCL sample improved the corrosion resistance drastically compared to the GE/PCL specimen. In vitro bioactivity of samples was examined after soaking the specimens for 7, 14 and 28 days in simulated body fluid (SBF). The results showed a significant apatite formation on the surface of 3BG/GE/PCL samples. The cell viability evaluation was performed using 3- (4, 5-dimethylthiazol-2-yl)-2,5 diphenyltetrazoliumbromide (MTT) tests which confirmed the enhanced cell viability on the surface of 3BG/GE/PCL samples. The in vivo behavior of specimens illustrated no toxicity and inflammatory response and was in a good agreement with the results obtained from the in vitro test.

Keywords: PCL; gelatin; bioglass; corrosion resistance; electrospinning; metallic implant

1. Introduction

AISI 316L Stainless Steel implants has been extensively used as orthopedic implants, dental implants, and cardiovascular stents due to its suitable mechanical properties, workability, high corrosion resistance, chemical stability, and low cost [1]. However, low biocompatibility, localized corrosion problems, and the release of Ni, Cr, and Mo ions from 316L SS can lead to immunoreactions and inflammatory responses, stimulate the platelet-activation, and provoke intimal hyperplasia [2]. Therefore, surface modification of 316L SS has been the topic of many research activities around the world [3–5]. Several techniques such as chemical modification, ion implantation, anodic oxidation,

physical vapor deposition, chemical vapor deposition, plasma spray deposition, sol-gel, thermal oxidation, and applying a composite coating have been utilized to modify the surface of 316L SS [6]. Among them, applying a composite coating is a simple, economical and effective method to improve the corrosion resistance and bioactivity of 316L SS substrates [7,8]. Various synthetic and natural polymers have been utilized for the surface modification of metallic implants [9,10]. Polycaprolactone (PCL) and gelatin are some examples of synthetic and natural polymers that have been used extensively in tissue engineering applications [11–15]. PCL is hydrophobic and is considered as a nontoxic and biodegradable polymer with a slow degradation rate, significant toughness, and remarkable mechanical properties. However, it has several disadvantages if applied as a coating material alone, including insufficient strength and the lack of desired bioactivity [13–15].

Within natural polymers, proteins have attracted considerable attention from scientists [16]; gelatin is a protein-based biopolymer that is formed by the chemical denaturation of collagen extracted from an animal's skin, bone or tissue [17]. Gelatin is of great interest due to its appropriate rheological film-forming properties, solubility in water, nontoxicity and gel-production capability at low concentrations [5]. However, it exhibits poor mechanical properties and a high degradability rate in the simulated body fluid (SBF) solution [18]. Studies have shown that the mechanical properties and stability of gelatin can be improved when mixed with other polymers. For example, gelatin/PCL composites could improve the biological performances and physical properties of the coatings [19–21]. On the other hand, 58S bioglass is a well-known material for its excellent bioactivity [22]. It has been reported that better mechanical properties and bioactivity can be achieved by compositing the bioglass (BG) in polymer coating. Khosravi et al. [23] investigated the effects of a poly (ε-caprolactone)/gelatin/forsterite coating containing a graphene oxide layer on the bioactivity, biodegradability and cell behavior of 316L Stainless Steel substrate. They found a higher bioactivity in the electrospun nanofibers containing 1 and 3 wt.% of forsterite nanoparticles after soaking in the SBF. The results of the MG-63 cell culture on the coatings showed an excellent cell adhesion along with considerable cell growth and proliferation on all samples. They reported that the presence of the forsterite nanoparticles and the graphene oxide layer substantially improved the cell proliferation of the coatings.

Different techniques have been utilized to produce nanobioglass/polymer composite coatings for stainless steel substrates, including electrodeposition, sol-gel, dipping, and spraying methods [24,25]. Among these procedures, the electrospinning process is one of the best techniques that utilizes electrical forces to produce ultrafine polymer fibers that mimic the natural cell environment. This method can be applied for soluble or fusible polymers alone or polymers containing particles or enzymes. The produced nanofibers exhibit many interesting features, such as a high surface area and tailorable porosity [26–28].

Coating 316L SS implants with biodegradable composite fibers to improve cell adhesion and bioactivity and to decrease the corrosion rate is quite a new approach, with only a few examples in the literature [29–32]. Despite the wide application of PCL/gelatin blended polymers, to the best of the authors' knowledge, applying GE/PCL including bioglass particles (BG/GE/PCL) composite coatings on 316L SS as the bone implant has not been investigated. In this study, a dip coating–electrospinning process was applied to coat the 316L SS substrates. The protective function of BG/GE/PCL composite coatings against corrosion was examined by electrochemical impedance spectroscopy (EIS) and potentiodynamic polarization. In addition, PCL-10 wt.% gelatin (GE/PCL) containing different amounts of bioglass particles was analyzed using XRD, SEM and energy-dispersive X-ray spectroscopy (EDS) techniques. Moreover, in vitro bioactivity of the coated samples was evaluated using SBF solution and 3-(4, 5-dimethylthiazol-2-yl)-2,5-diphenyltetrazoliumbromide (MTT) analysis. Finally, the in vivo study was carried out by implanting the bare and coated 316L SS substrates in rabbits. The results suggested that incorporating bioglass particles as a reinforcement in the GE/PCL matrix can enhance surface roughness, corrosion resistance and bioactivity of the coated samples.

2. Materials and Methods

2.1. Synthesis of Bioglass Nanopowder

The 58S bioactive glass nanopowder was produced with the composition of 57.72 mol.% SiO_2, 35.09 mol.% CaO, and 7.1 mol.% P_2O_5 using the sol-gel technique. To produce the bioglass powder, a solution containing 17.5 mL of 2 M hydrochloric acid in deionized water, 50 mL ethanol, 20.5 mL tetraethyl orthosilicate (TEOS) and 2 mL triethyl phosphate (TEP) were prepared. Then, 15 wt.% calcium nitrate ($Ca(NO_3)_2{\cdot}4H_2O$) was added to the solution. The suspension was magnetically stirred for 1h and subsequently aged at 60 °C in an oven for 54 h. After aging, the suspension dried at 130 °C for 72 h, and finally calcined at 1100 °C for 1h. The obtained bioglass powder was mechanically agitated for 1 h in a planetary ball mill (PM100) under ambient conditions. The milling media consisted of a zirconia vial with five 20 mm zirconia balls. In all milling runs, the ball-to-powder weight ratio was 10:1 and the rotational speed of the main disc was 250 rpm.

2.2. Fabrication of PCL-10 wt.% Gelatin–Bioglass Composite Coatings

Commercial 316L stainless steel specimens with dimensions of $10 \times 10 \times 2$ mm^3 were wire cut and mechanically polished using SiC papers (up to 2000) and ultrasonically cleaned with distilled water/acetone solution at 25 °C. Subsequently, the specimens were chemically activated by immersion in a solution containing a 30:70 volume ratio of H_2O_2:HNO_3 for 30 s to improve the adhesion of the coating to the substrate.

On the other hand, the polymer–ceramic composite coating of PCL-10 wt.% gelatin (GE/PCL) was initially prepared by stirring a mixture of PCL (70–90 $\times$ 10^3 g/mol, Sigma-Aldrich) and gelatin in a formic acid/acetic acid solution for 4 h at 25 °C. Subsequently, various amounts of bioglass (BG) (1, 3 and 5 wt.%) were added to the GE/PCL solution, stirred for 1 h and ultrasonicated for 30 min to disperse nanoparticles in the polymeric solution. Table 1 shows the designation of different samples. The 316L SS specimens were soaked in GE/PCL solution for 2 min and then dried for 1 min. This process was repeated 5 times to achieve a proper thickness for the base coat. Subsequently, the electrospinning technique was utilized to apply the GE/PCL containing different amounts of bioglass nanocomposite coating on the surface of 316L SS specimens as the topcoat. The electrospinning method was carried out according to [33]. Sample preparation was performed at room temperature with 30% humidity. The voltage of the system was adjusted to 12 kV. The volumetric flow rate of syringe was set to 5 mL/h and it was placed with the distance of 15 cm from the metallic substrate.

Table 1. Designation and specification of different samples.

Designation	Polycaprolactone (wt.%)	Gelatin (wt.%)	Bioglass (wt.%)
GE/PCL	90	10	-
1BG/GE/PCL	89.1	9.9	1
3BG/GE/PCL	87.3	9.7	3
5BG/GE/PCL	85.5	9.5	5

2.3. Characterization of the Nanofibrous Composite Coating

The topography of the surface of samples was analyzed using scanning electron microscopy (SEM, model Philips XL30, Eindhoven, The Netherlands). SEM was also utilized to observe bioglass nanopowder distribution in the composite coating. Phase analysis of the surface of samples was investigated by X-ray diffraction (XRD, Philips X'pert MPD, Eindhoven, The Netherlands, Cu Kα at 40 kV and 30 mA) in a 2θ range of 10°–90° with a step size of 0.05° per sec. The chemical composition of the surface of specimens was determined using energy-dispersive X-ray analysis (EDS, AIS 2300C, Seron, South Korea). To measure the surface roughness of the composite, a laser surface profilometer was used and the average roughness values (R_a) of various samples were recorded. The adhesion

strength of the composite coating to the substrate was investigated using the pull-off test by applying and removing pressure-sensitive tape according to the American Society of Testing and Materials (ASTM) test protocol D3359 [5].

2.4. Electrochemical Evaluation

To observe the corrosion behavior of the composite coating in the body, an electrochemical evaluation was performed in phosphate-buffered saline (PBS) solution made by using Cold Spring Harbor Protocol [34], containing 137 mM/L NaCl, 2.7 mM/L KCl, 10 mM/L Na_2HPO_4 and 1.8 mM/L KH_2PO_4 at the temperature of (37 °C) and pH = 7.4. The electrochemical behavior was determined by electrochemical impedance spectroscopy (EIS) using an Ivium potentiostat. A conventional three-electrode arrangement was used with a KCl saturated calomel electrode (SCE) as a reference electrode. A platinum sheet was utilized as a counter electrode and the 316L SS coated specimens were used as the working electrodes. The electrodes were kept in PBS solution for 30 min to be stabilized at open circuit potential (OCP) before electrochemical evaluation. The EIS measurements were conducted with the frequency range of 100 kHz–10 mHz and amplitude of 10 $mV{\cdot}rms^{-1}$.

2.5. In Vitro Study

Simulated body fluid (SBF) solution with ion concentration close to that of human blood plasma was used to investigate the bioactivity of the specimens as described in [35]. The apatite formation capability of the bare 316L SS and 3BG/GE/PCL samples was evaluated by soaking the specimens in SBF at pH 7.4 for 7, 14 and 28 days. The SBF solution was prepared according to the protocol presented in [35] including 142.0 mM Na^+, 5.0 mM K^+, 1.5 mM Mg^{2+}, 2.5 mM Ca^{2+}, 125.0 mM Cl^-, 27.0 mM $HCO_3{}^-$, 1.0 mM $HPO_4{}^{2-}$ and 0.5 mM $SO_4{}^{2-}$. After immersing the samples for 7, 14 and 28 days, the samples were gently rinsed with double deionized water and dried at room temperature. The samples were analyzed by SEM and (EDS).

2.6. Cell Culture and Cell Viability Study

Biological characterization of the samples was studied using MG63 human osteoblast-like cells (CRL-1427, 17 years, Caucasian, passage 4). MG63 were cultured in (Gibco Dulbecco's Modified Eagle Medium) DMEM-low glucose including 10% (*v*/*v*) streptomycin/penicillin (bioidea, Tehran, Iran) inside an incubator at 37 °C under 5% CO_2. In addition to culture medium refreshing, phosphate buffer saline solution (PBS, bioidea, Tehran, Iran) was selected to wash the culture plates. Furthermore, plates were sterilized for 60 min in 70% (*v*/*v*) ethanol and 6 h under UV light. After immersing the samples in culture medium for one day, and as soon as the cell confluence reached 70%, the cells were trypsinized with a density of 30,000 cells/well and sealed on tissue culture plate (TCP) and then incubated at 37 °C and 5% CO_2. The cell proliferation was evaluated using MTT assay. For this purpose, samples were placed in cell medium and after 1, 3 and 5 days, the culture medium was removed and MTT solution with 0.5 mg/mL regent was added to the samples as well as the control specimens. At the next level, before adding DSMO, the samples were incubated at 37 °C and 5% CO_2 for 4 h. Incubation at 37 °C and 5% CO_2 was repeated to dissolve the dark blue formazan crystals. Afterwards, the DMSO absorption was measured at 570 nm wavelength by employing a microplate reader and finally the relative cell culture of the samples reported according to the following equation [36,37]:

$$\text{Relative cell survival (\% control)} = \frac{\left(X_{\text{sample}} - X_{\text{b}}\right)}{\left(X_{\text{c}} - X_{\text{b}}\right)} \times 100 \quad (1)$$

where X_{sample}, X_{b} and X_{c} are absorbance of the sample, blank (DMSO) and control (TCP), respectively.

2.7. In Vivo Study

In this study, five adult male New Zealand white rabbits weighing 1–1.5 kg were utilized for in vivo study. This experiment was approved by the School of Dentistry at Isfahan University of Medical Sciences. General anesthesia was induced by Ketamine hydrochloride (50 mg/kg body weight) and Acepromazine (1 mg/kg body weight) injection. After anesthesia, Flunex (0.6 mg/kg) was injected under the skin of the rabbits. Afterward, the surgical areas were shaved, and their skin was washed with chlorhexidine and povidone–iodine and marked. The 3BG/GE/PCL samples were sterilized by immersion in 70% (*v*/*v*) ethanol and then exposed to UV light for 6 h [33]. The surgical sites on the skin were exposed with an incision using a scalpel and the samples were implanted under the skin. The control and coated samples were implanted for up to 90 days. Afterwards, the location of the surgery was closed using Nylon suture. To control pain and infection, Flunex drug (0.6 mg/kg body weight, every 24 h) and penicillin (6000 mg/kg body weight, every 8 h) were injected, respectively. Specimens were received in 10 formalin and then tissue processing was performed. The tissue processing steps were fixation (with formalin), dehydration (through grades of alcohol 70, 80 and 90% and absolute alcohol), clearing (xylene), impregnation, embedding and blocking (tissue cutting with microtome measuring 3–5 mm), section cutting and hematoxylin and eosin (H&E) staining, respectively [38–40]. The sections were studied by a pathologist.

3. Result and Discussion

3.1. Surface Morphology and Elemental Analysis of BG/GE/PCL Composites

Figure 1 shows the morphology of the BG/GE/PCL composites. The SEM results showed a porous structure with randomly oriented features throughout the BG/GE/PCL nanofibrous coatings. The average diameter of the BG/GE/PCL nanofibers was around 200 nm. The porosity of the BG/GE/PCL composite coating provided a large surface area to volume ratio for cell attachment, as well as adequate space for bone ingrowth. A smooth and bead-free morphology with uniform fiber diameter and appropriate porosity was obtained in the BG/GE/PCL composite coatings. Increasing the amount of bioglass in the composite coating resulted in the formation of large particles in the 5BG/GE/PCL sample.

The presence of bioglass particles in the 3BG/GE/PCL composite coatings was investigated using EDS analysis (Figure 2). Ca, P, and Si peaks were detected in the EDS graph, which proved the presence of bioglass particles in the composite coatings (Figure 2b). The carbon peak shown in the EDS graph can be assigned to the presence of both PCL and Gelatin in the composite coating. Oxygen peaks, which were originated from PCL, gelatin and bioglass, were also detected in the EDS analysis. An N peak was related to the gelatin in the composite coating. EDS chemical maps were acquired to determine the distribution of Si, Ca, P, and N elements in the 3BG/GE/PCL composite. Figure 2c shows a typical elemental map of Si, Ca, P, and N. Although bioglass was well dispersed throughout the material, pockets of bioglass were detected as well. As can be seen, all elements were homogeneously distributed in the composite. It should be mentioned that the homogenous distribution of bioglass particles is very important in the bioactivity of the composites. As seen, by increasing the amount of bioglass to 3 wt.%, there was a proper and uniform distribution of bioglass in the 3BG/GE/PCL sample; however, a further increase to 5 wt.% (5BG/GE/PCL sample) caused the formation of agglomerates and bioglass pockets in the coating.

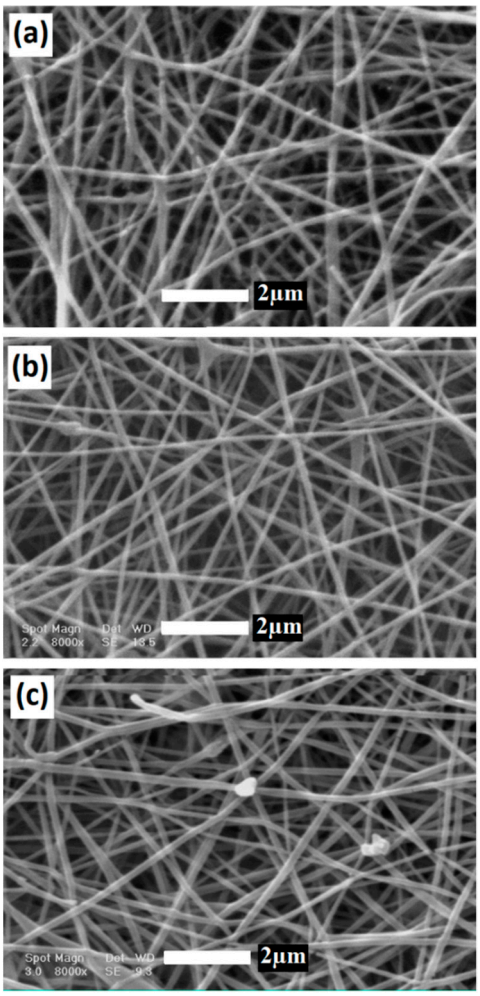

Figure 1. SEM micrographs of (**a**) 1BG/GE/PCL, (**b**) 3BG/GE/PCL and (**c**) 5BG/GE/PCL composites.

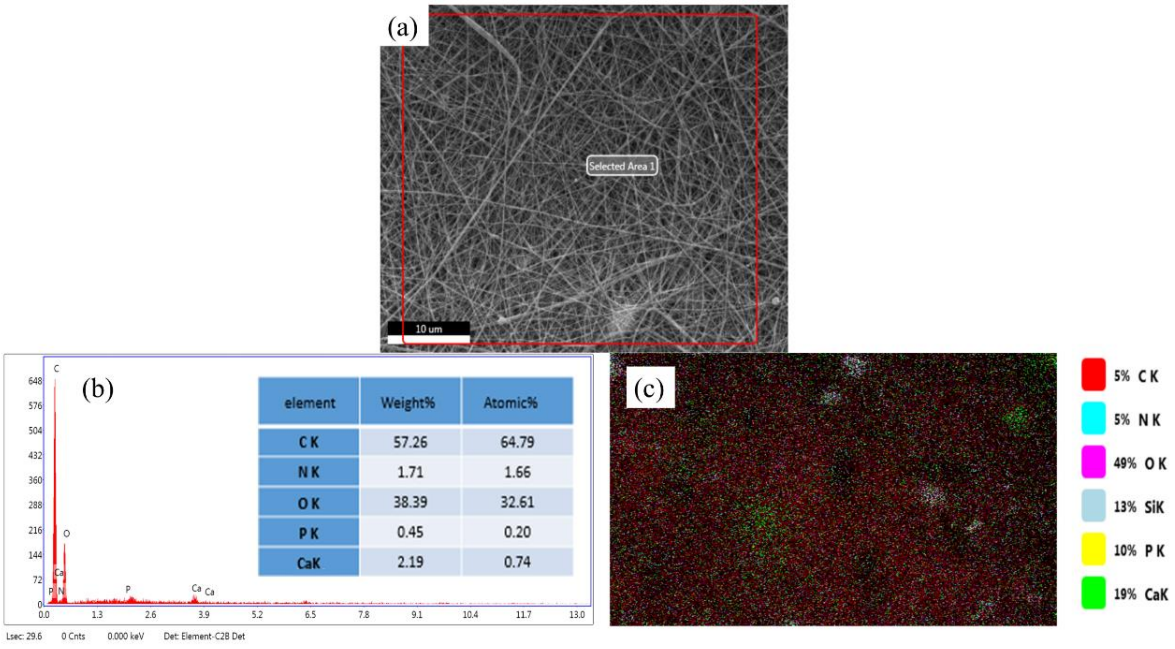

Figure 2. (**a**) SEM (**b**) Energy-dispersive X-ray spectroscopy (EDS) area analysis and (**c**) EDS map analysis of the 3BG/GE/PCL composite coating.

3.2. Phase Analysis

The XRD patterns of different composite coatings are illustrated in Figure 3. The characteristic peaks of PCL were observed in GE/PCL samples at 2θ equal to 22.2°, 23.5°, 25.5° and 36.9°, which belong to the (011), (210), (120) and (311) crystallography planes (JCPDS card number 48-2219), respectively. On the other hand, the intensity of characteristic peaks of PCL was decreased in the BG/GE/PCL composite as a result of the presence of bioglass in the structure. The characteristic peaks of bioglass in the 1BG/GE/PCL composite were negligible in the XRD patterns due to the low amount of bioglass in the structure and it probably being in the amorphous state. Some additional peaks were observed at around 2θ equal to 43.5°, 50.7° and 74.7° due to the presence of 316L SS substrate (JCPDS card number 33-0397) [41]. By increasing the bioglass content in the coating, the intensity of the SS XRD peaks decreased due to the formation of a thicker coating on the substrate.

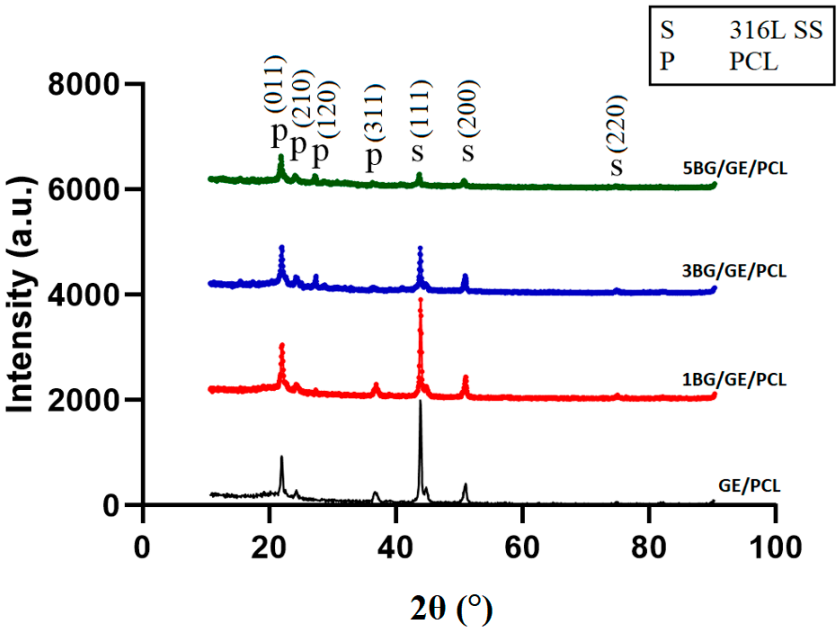

Figure 3. The XRD patterns of GE/PCL and BG/GE/PCL composites.

3.3. Surface Roughness and Adhesion Strength of the Coated Samples

The surface coating of implants influences osteoblastic proliferation and differentiation. The fixation of a metallic implant to the bone tissue is affected by various factors, including surface roughness. After implantation, the implant surface is in contact with body fluid and interacts with different types of cells. It has been confirmed that increasing the surface roughness may lead to cell adhesion and bone formation on the surface of metallic implants [42,43]. The results of the surface roughness are summarized in Table 2. As can be seen, by increasing the amount of embedded bioglass in GE/PCL, the surface roughness of the samples increased. Figure 4 shows the surface roughness profiles of different samples. Increasing the weight percentage of bioglass in the composite coatings increased the surface roughness. The adhesion strength of the composite coatings was evaluated according to the D3359-ASTM standard [44,45]. The composite coatings in the 3BG/GE/PCL and 5BG/GE/PCL samples showed the strongest adhesion to the substrate with a rating of 6B. The removed area of the composite coating was less than 4B, which demonstrated a proper coating adhesion to the substrate. Table 3 shows the results of the adhesion strength of different samples. As can be seen, by increasing the amount of bioglass in the composite coating, the adhesion strength was improved. The minimum adhesion strength was observed in the samples without the bioglass particles. Bioglass nanopowders act as pins in the composite coating, which cause greater surface roughness and adhesion strength. It seems that incorporating the bioglass nanoparticles to the GE/PCL composite increased the

contact surface area of the coating to the substrates. Torkaman et al. [21] reported that adding forsterite bioceramic powder particles into the polymer matrix could increase the surface adhesion of the coating to the substrates. Furthermore, it is reported that adding BG submicron particles to the PCL coating can improve its interfacial adhesion and its wettability [46]. The increased surface roughness of the coating may increase the contact points and subsequently raise the adhesion strength of the coating. As seen in Figure 1, increasing the amounts of the bioglass from 3 to 5 wt.% in the composite coating resulted in the formation of large particles and an inhomogeneous structure. Considering the surface roughness, homogeneous distribution of the bioglass in the coating and the adhesion strength of various coatings, 3BG/GE/PCL samples were used as the optimum specimens to evaluate the electrochemical behavior and bioactivity compared to GE/PCL samples.

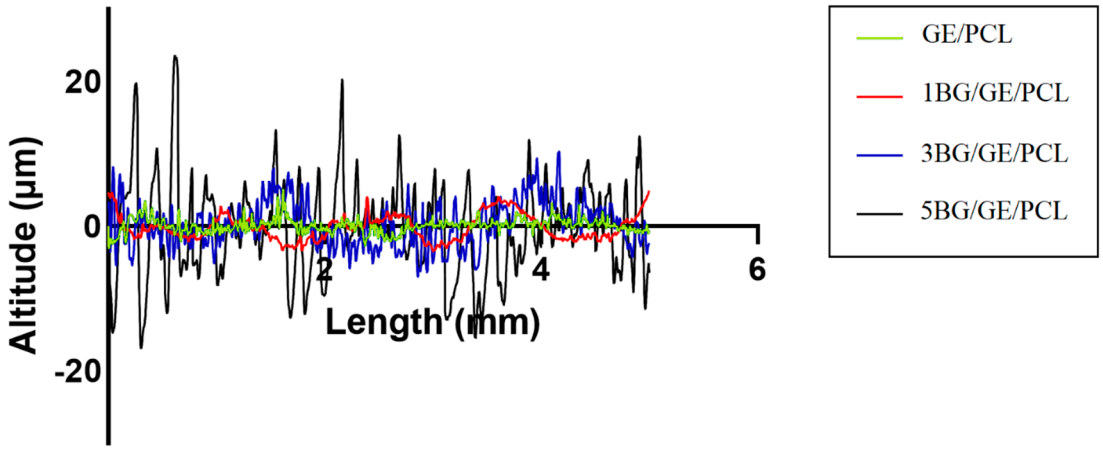

Figure 4. The surface roughness diagram of different samples.

Table 2. The results of the surface roughness of different samples.

Samples	Surface Roughness (μm)		
	R_a (the Average Roughness)	R_q	R_z
5BG/GE/PCL	5.08	6.62	40.37
3BG/GE/PCL	2.57	3.16	17.26
1BG/GE/PCL	1.47	1.78	8.65
GE/PCL	0.71	0.97	8.09

Table 3. The adhesion strength of different samples.

Samples	Classification	% of Area Removed
5BG/GE/PCL	6B	Less than 5%
3BG/GE/PCL	6B	Less than 5%
1BG/GE/PCL	3B	5–15%
GE/PCL	3B	5–15%

3.4. Electrochemical Behavior of Coated Substrates

The Nyquist plots, the equivalent circuit used to simulate the EIS experimental data, and the Bode-Z and Bode-phase diagrams of GE/PCL and 3BG/GE/PCL samples in a PBS solution are presented in Figure 5. The Nyquist plots (Figure 5a) are described by an equivalent circuit (EC) that has two time-constants (Figure 5b). This EC has also been used for a forsterite/GE/PCL nano composite coating applied onto a titanium substrate [33]. The R_s is considered as solution resistance, CPEcoat and *R*coat as constant phase element of coating and coating resistance, and CPEdl and *R*ct as constant phase elements of double layer and charge transfer resistance [47]. Table 4 shows the circuit parameters calculated using z-view software. The diameter of the semicircle of 3BG/GE/PCL coating in the Nyquist

plots is larger than that of GE/PCL coating, which demonstrates an increase in the corrosion resistance of the polymer coating containing bioglass particles. Although PCL is a hydrophobic polymer, adding BG nanoparticles to the PCL polymer matrix can improve the hydrophilicity of the polymer coating [46]. The increased hydrophilicity caused a better attachment of the coating to the substrate and consequently provided a better protective layer on the surface of substrate against corrosion. The *R* (both *R*coat and *R*ct) values in the 3BG/GE/PCL coating are significantly higher than GE/PCL coating which proved the higher corrosion resistance through adding 3BG to the GE/PCL coating. The *R*ct of 3BG/GE/PCL reached the value of 49,634 kΩ·cm^2, approximately five times more than that of the GE/PCL sample. The better attachment of the 3BG/GE/PCL coating to the substrate postponed the contact between corrosive ions such as Cl^- and the substrate, and subsequently caused the degradation which occurs over a longer period [48]. Increasing the impedance of the superhydrophobic coating reduced the metals' dissolution and the suppression of oxygen reduction activity by the BG/GE/PCL coating. In the equivalent circuits, Rs, had approximately the same value for both the aforementioned samples. Because the capacitance had deviated from its ideal capacitive behavior, the constant phase element (CPE) was utilized to substitute Cdl with Qdl in the equivalent circuit. The value of n ranging from 0 to 1 was related to the surface roughness; where $0.5 < n < 1$. The deviation of the samples from the ideal behavior could be ascribed to the surface roughness of electrode, to a nonhomogeneous current distribution on the electrode surface or to a non-homogenous distribution of the electrical properties within the coating which was ascribed to the superhydrophobic nature of the nanocomposite coating [49,50].

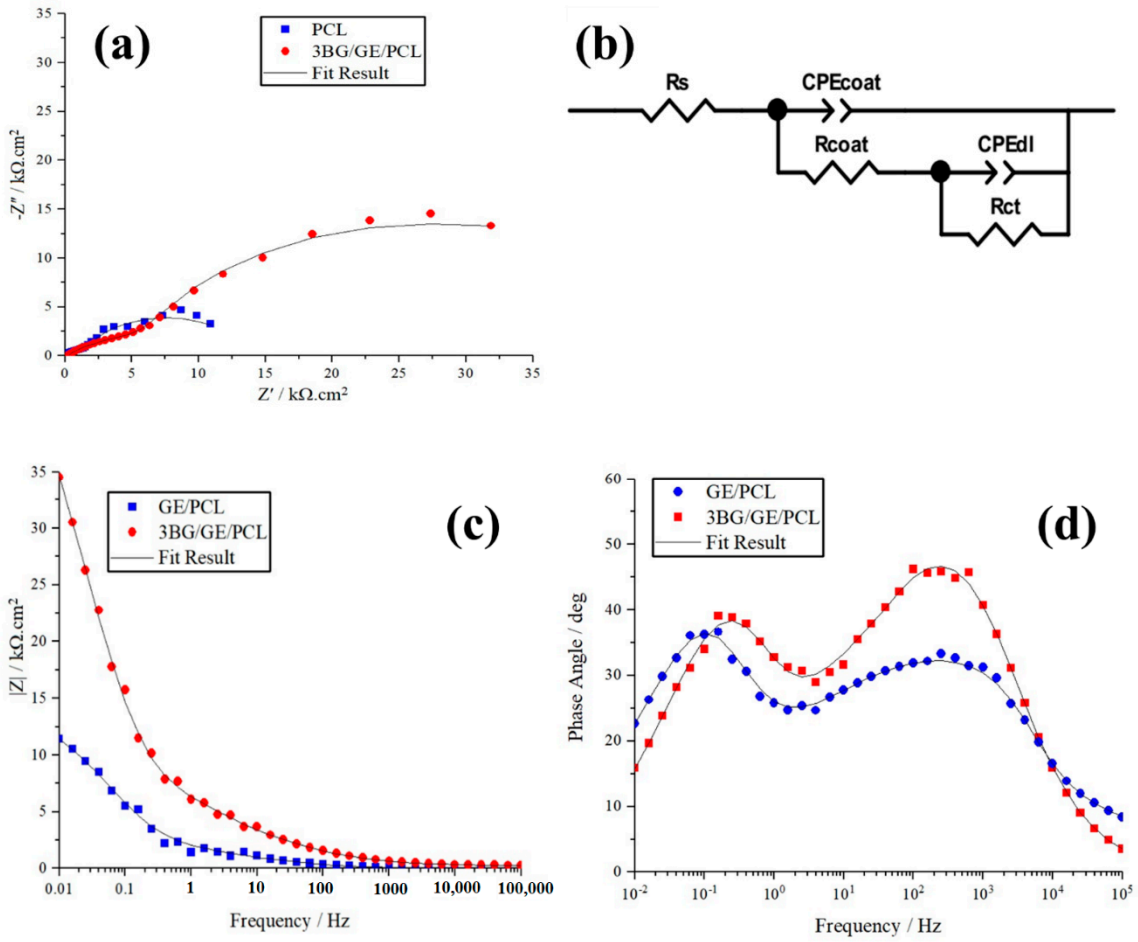

Figure 5. (**a**) Nyquist plots, (**b**) the equivalent circuit used to simulate the electrochemical impedance spectroscopy (EIS) experimental data, (**c**) the Bode-Z and (**d**) Bode-phase diagrams of 3BG/GE/PCL and GE/PCL in a PBS solution at room temperature.

Table 4. The circuit parameters of EIS results of PCL-10 wt.% Gelatin-1,3 and 5% Bioglass composite calculated using z-view software (version 3.1) in a PBS solution at room temperature.

Samples	R_s ($\Omega\,cm^2$)	CPEcoat ($\mu F{\cdot}cm^{-2}$)	n	Rcoat ($\Omega{\cdot}cm^2$)	CPEdl ($\mu F{\cdot}cm^{-2}$)	n	Rct ($\Omega{\cdot}cm^2$)	χ^{-2} (Chi-Squared)
GE/PCL	41.56	9.37×10^{-5}	0.72	2141	1.21×10^{-4}	0.89	11,543	0.00028
3BG/GE/PCL	45.4	6.52×10^{-5}	0.43	10,790	1.21×10^{-7}	0.86	49,634	0.00027

The Bode-Z and Bode-phase diagrams of the 3BG/GE/PCL and GE/PCL samples in a PBS solution at room temperature are shown in Figure 5c,d, respectively. As seen in the Bode-Z curve, the resistance at high-frequencies and low-frequencies was related to the characteristic of protective coating and quality of the inner surface of the barrier coating at the coating–substrate interface, respectively. The 3BG/GE/PCL sample drastically increased the resistance at low frequencies, proving the significant improvement in the protective properties and corrosion resistance of the coating. In addition, regarding the Bode-phase diagram, there are two time-constants, one at the mid-frequencies and another at low frequencies in both samples. At low frequencies, the phase angle of GE/PCL sample was about −30°, while in 3BG/GE/PCL sample it was about −50°. In addition, the phase angle increased from about −35° for GE/PCL to about −40° for 3BG/GE/PCL at the mid-frequencies, indicating an improvement in the corrosion resistance of the coating. The 3BG/GE/PCL coating could reduce the corrosive process and protect the metal substrate from PBS ion attacks. In general, the EIS curves showed that the corrosion resistance of 3BG/GE/PCL sample increased compared to the GE/PCL specimen due to a decrease in the electron transfer in the coating containing bioglass particles.

3.5. Bioactivity Evaluation

The ability of implant surface to improve the nucleation and growth of bone-like hydroxyapatite upon immersion in SBF is a common method to evaluate the bioactivity and osteoconductivity of the surface [51]. The 3BG/GE/PCL samples were soaked in SBF solution for various times to investigate the hydroxyapatite formation on the coated samples. The SEM micrographs and EDS analysis of 3BG/GE/PCL samples after immersion in SBF are presented in Figure 6. The SEM micrographs of the coated samples after soaking in SBF solution revealed the presence of spherical-like particles. The EDS analysis (Figure 6e) showed that these spherical particles contained Ca, P, and O elements, proving the formation of hydroxyapatite on the surface of the samples after immersion in the SBF solution. The 3BG/GE/PCL samples showed significant precipitation of hydroxyapatite on the coating surface. By increasing the immersion time from 7 to 28 days, the density of apatite deposited on the 3BG/GE/PCL samples increased. This could be due to the degradation of bioglass and the formation of local supersaturation of calcium and phosphate ions on the surface of samples [52–54]. Subsequently, more hydroxyapatite particles appeared on the surface of the samples. In addition, adding BG to the coating resulted in an increase in its wettability [46] and enhanced water uptake, which improved the calcium absorption from the SBF solution and therefore the bioactivity of the samples.

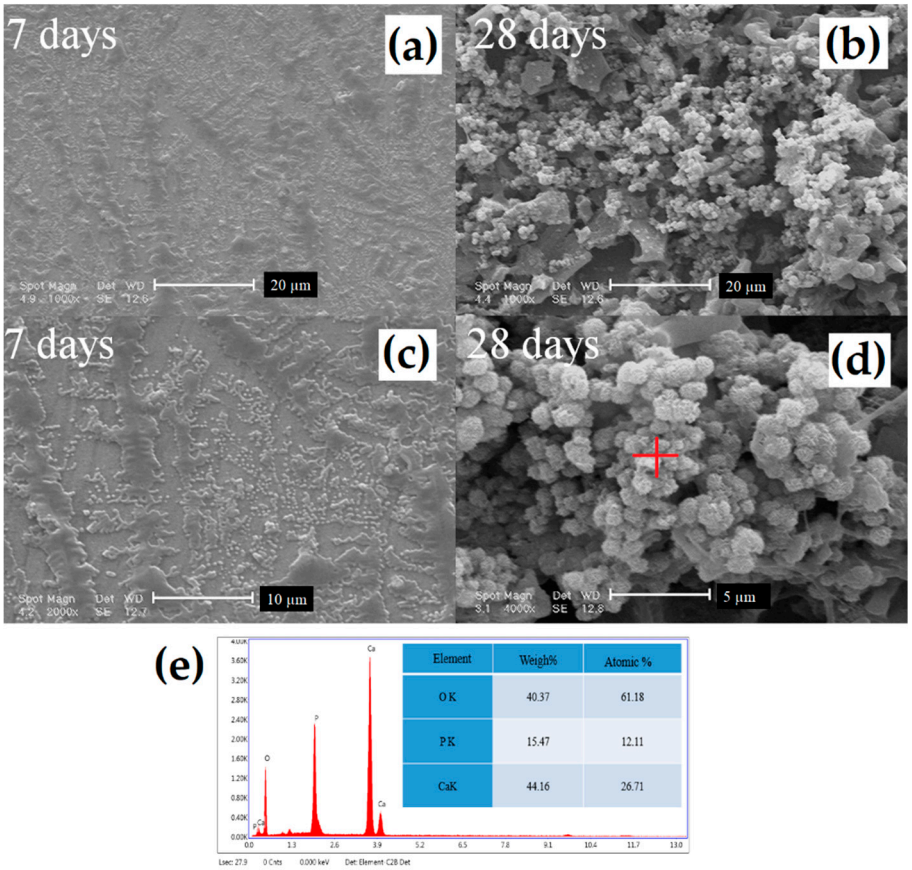

Figure 6. SEM micrographs of the surface of 3BG/GE/PCL samples after soaking in SBF solution for (**a**,**c**) 7 days and (**b**,**d**) 28 days. (**e**) The EDS results of the 3BG/GE/PCL sample after 28 days of immersion in the SBF solution.

3.6. MTT Analysis

To assess the biocompatibility of the 3B/GE/PCL sample, an MTT assay was performed. MTT assays provide a quantitative assessment of the cellular response to the surface of coated substrates [55–57]. The results of cell viability illustrated in Figure 7 were determined by the cell counting method [58]. The cell viability of the GE/PCL and 3BG/GE/PCL samples was measured after one, three, and seven days of cell culture. As observed, the number of cells increased with the increasing in the incubation time for 3BG/GE/PCL. After one day of cell culture, small differences in cell proliferation between the GE/PCL and 3BG/GE/PCL sample were observed. This could be attributed to the fact that MG63 cells try to adapt to the sample surface. After three days of MG63 cell culture, the surface of 3BG/GE/PCL samples demonstrated a higher level of proliferation compared to the GE/PCL. This proliferation promoted bone extracellular matrix activity, and consequently the growth rate. By increasing the time of cell culture to seven days, further cell proliferation was observed on the surface of the 3BG/GE/PCL samples. This increase in the cell viability and cell proliferation can be ascribed to the increase in surface roughness in the 3BG/GE/PCL samples compared to the GE/PCL specimens. In addition, the presence of bioglass in the coating led to an increase in the hydrophilicity nature of samples which resulted in an increase in the cell viability of 3BG/GE/PCL samples.

3.7. In Vivo Study

In this research, the in vivo behavior of different implants (3BG/GE/PCL samples as well as bare 316L SS) was studied. Figure 8 shows the surface of uncoated and coated substrates after 90 days of implantation. Compared to bare 316L SS, the 3BG/GE/PCL sample did not show any inflammation or granulation tissue, endothelial swelling, or fibrotic tissue. No rejection was observed in the 3BG/GE/PCL

samples, which proved its ability for cell attachment. Furthermore, the histologic findings proved the bioavailability of the coated samples.

In the coated samples, there was no evidence of inflammation or toxicological effects. The absence of any inflammation, fibrosis or granulation tissue can confirm the non-toxicity of the 3BG/GE/PCL implants. In addition, some areas in the coated implants showed local calcification, which is a sign of faster ossification in these samples (Figure 8d,e). The designated areas (white rectangle) showed the initial formation of fibrous tissue, which was an extracellular matrix. Ossification is a prolonged process and other techniques can be applied to better study the ossification [59,60].

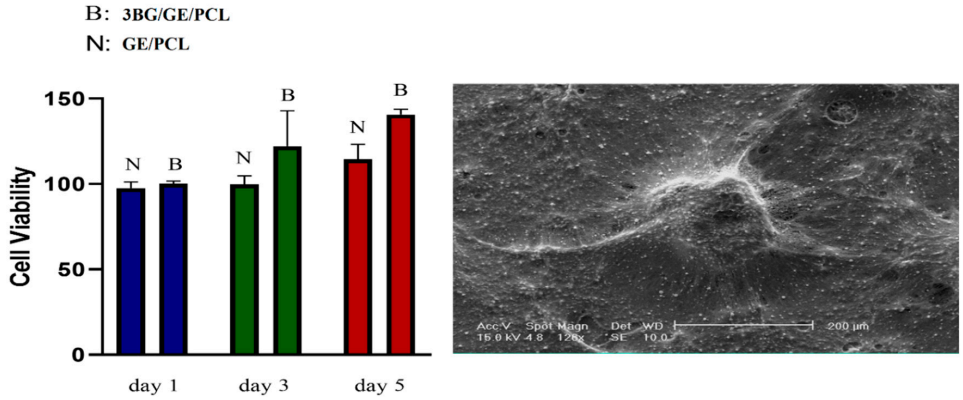

Figure 7. MTT assay on 3BG/GE/PCL samples as well as the results of cell viability determined by the cell counting method.

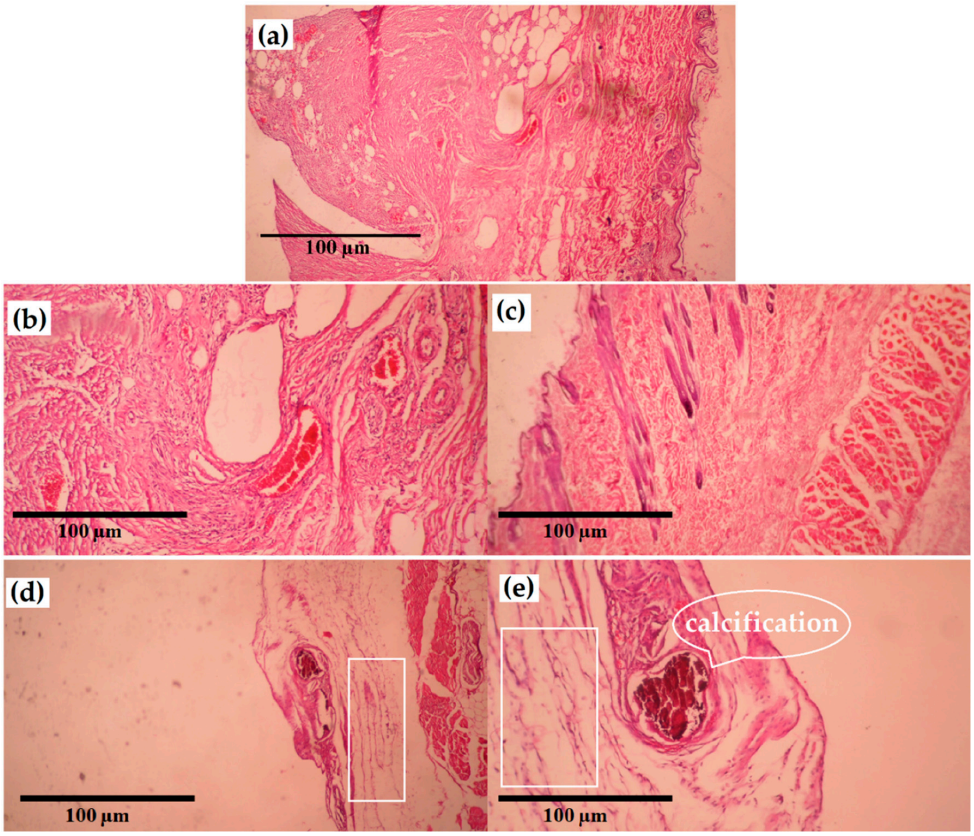

Figure 8. (**a**) Hematoxylin and eosin (H&E) staining of uncoated implants. No evidence of inflammation, fibrosis, or necrosis. The histologic findings are the confirmed bioavailability of coated implants; (**b**,**c**) (H&E) staining of coated implants. No evidence of inflammation or fibrosis (rejection criteria is not seen and bioavailability is confirmed); (**d**,**e**) Focal area of calcification in coated implants.

4. Conclusions

In this study, we developed GE/PCL and BG/GE/PCL nanocomposite coatings on the surface of 316L SS substrates by utilizing dip coating and electrospinning techniques. SEM results showed that BG/GE/PCL fibers had an average diameter of less than 200 nm. There was a growth in both the surface roughness and the adhesion strength by increasing the amount of bioglass from 1 to 3 wt.% in the coating. The corrosion behavior of different coatings was characterized by EIS in the PBS solution. The corrosion resistance of the 3BG/GE/PCL sample was higher than that of GE/PCL. More importantly, the 3BG/GE/PCL specimen showed higher bioactivity. Furthermore, MTT analysis revealed that the presence of bioglass in the 3BG/GE/PCL specimen increased the cell viability compared to the GE/PCL sample. The in vivo results in the animal model demonstrated no inflammation or granulation tissue, endothelial swelling, fibrotic tissue, or toxicological effect in the 3BG/GE/PCL sample, which was in a good agreement with the in vitro results. The results showed that the nanofibrous composite coating can improve the corrosion resistance, cell viability and bioactivity of the 316L SS implant, and could be a promising composite for orthopedic applications.

Author Contributions: Conceptualization, B.M.S., R.T., M.M., and R.E.; methodology, B.M.S., R.T., and R.E.; validation, B.M.S., R.T., and M.M.; formal analysis, B.M.S., R.T., and M.M.; investigation, B.M.S., R.T., and R.E.; resources, R.T. and M.M.; writing—original draft, B.M.S., R.T., M.M., R.E., M.D., and F.T.; writing—review and editing, R.E., M.D., E.K., and F.T.; visualization, B.M.S., R.T., M.M., R.E., and F.T.; supervision, R.E. and F.T.; project administration, B.M.S., R.E., and F.T. All authors have read and agreed to the published version of the manuscript.

Funding: This research received no external funding.

Conflicts of Interest: There is no conflict of interest.

References

1. Bordjih, K.; Jouzeau, J.-Y.; Mainard, D.; Payan, E.; Delagoutte, J.-P.; Netter, P. Evaluation of the effect of three surface treatments on the biocompatibility of 316L stainless steel using human differentiated cells. *Biomaterials* **1996**, *17*, 491–500. [CrossRef]
2. Talha, M.; Behera, C.; Sinha, O. Effect of nitrogen and cold working on structural and mechanical behavior of Ni-free nitrogen containing austenitic stainless steels for biomedical applications. *Mater. Sci. Eng. C* **2015**, *47*, 196–203. [CrossRef] [PubMed]
3. Gadkari, S.; Gu, S.; Sadhukhan, J. Two-dimensional mathematical model of an air-cathode microbial fuel cell with graphite fiber brush anode. *J. Power Sources* **2019**, *441*, 227145. [CrossRef]
4. Kocijan, A.; Conradi, M.; Hočevar, M. The influence of surface wettability and topography on the bioactivity of TiO_2/epoxy coatings on AISI 316L stainless steel. *Materials* **2019**, *12*, 1877. [CrossRef]
5. Vickers, N.J. Animal communication: When i'm calling you, will you answer too? *Curr. Biol.* **2017**, *27*, R713–R715. [CrossRef]
6. Bekmurzayeva, A.; Duncanson, W.J.; Azevedo, H.S.; Kanayeva, D. Surface modification of stainless steel for biomedical applications: Revisiting a century-old material. *Mater. Sci. Eng. C* **2018**, *93*, 1073–1089. [CrossRef]
7. Avcu, E.; Baştan, F.E.; Abdullah, H.Z.; Rehman, M.A.U.; Avcu, Y.Y.; Boccaccini, A.R. Electrophoretic deposition of chitosan-based composite coatings for biomedical applications: A review. *Prog. Mater. Sci.* **2019**, *103*, 69–108. [CrossRef]
8. Kubisztal, J.; Kubisztal, M.; Stach, S.; Haneczok, G. Corrosion resistance of anodic coatings studied by scanning microscopy and electrochemical methods. *Surf. Coat. Technol.* **2018**, *350*, 419–427. [CrossRef]
9. Alizadeh-Osgouei, M.; Li, Y.; Wen, C. A comprehensive review of biodegradable synthetic polymer-ceramic composites and their manufacture for biomedical applications. *Bioact. Mater.* **2019**, *4*, 22–36. [CrossRef]
10. Zahran, M.; Marei, A.H. Innovative natural polymer metal nanocomposites and their antimicrobial activity. *Int. J. Biol. Macromol.* **2019**, *136*, 586–596. [CrossRef]
11. Abrisham, M.; Noroozi, M.; Panahi-Sarmad, M.; Arjmand, M.; Goodarzi, V.; Shakeri, Y.; Golbaten-Mofrad, H.; Dehghan, P.; Sahzabi, A.S.; Sadri, M.; et al. The Role of Polycaprolactone-Triol (PCL-T) in Biomedical Applications: A state-of-the-art review. *Eur. Polym. J.* **2020**, *131*, 109701. [CrossRef]
12. Jia, L.; Han, F.; Wang, H.; Zhu, C.; Guo, Q.; Li, J.; Zhao, Z.; Zhang, Q.; Zhu, X.; Li, B. Polydopamine-assisted surface modification for orthopaedic implants. *J. Orthop. Transl.* **2019**, *17*, 82–95. [CrossRef] [PubMed]

13. Catauro, M.; Bollino, F.; Giovanardi, R.; Veronesi, P. Modification of Ti6Al4V implant surfaces by biocompatible TiO2/PCL hybrid layers prepared via sol-gel dip coating: Structural characterization, mechanical and corrosion behavior. *Mater. Sci. Eng. C* **2017**, *74*, 501–507. [CrossRef] [PubMed]
14. Catauro, M.; Bollino, F.; Papale, F.; Marciano, S.; Pacifico, S. TiO2/PCL hybrid materials synthesized via sol-gel technique for biomedical applications. *Mater. Sci. Eng. C* **2015**, *47*, 135–141. [CrossRef] [PubMed]
15. Grossen, P.; Witzigmann, D.; Sieber, S.; Huwyler, J. PEG-PCL-based nanomedicines: A biodegradable drug delivery system and its application. *J. Control. Release* **2017**, *260*, 46–60. [CrossRef] [PubMed]
16. Pokorski, J.K.; Hore, M.J. Structural characterization of protein–polymer conjugates for biomedical applications with small-angle scattering. *Curr. Opin. Colloid Interface Sci.* **2019**, *42*, 157–168. [CrossRef]
17. Lv, L.-C.; Huang, Q.-Y.; Ding, W.; Xiao, X.-H.; Zhang, H.-Y.; Xiong, L.-X. Fish gelatin: The novel potential applications. *J. Funct. Foods* **2019**, *63*, 103581. [CrossRef]
18. Govindan, R.; Gu, F.; Karthi, S.; Girija, E. Effect of phosphate glass reinforcement on the mechanical and biological properties of freeze-dried gelatin composite scaffolds for bone tissue engineering applications. *Mater. Today Commun.* **2020**, *22*, 100765. [CrossRef]
19. Divya, M.; Vaseeharan, B.; Abinaya, M.; Vijayakumar, S.; Govindarajan, M.; Alharbi, N.S.; Kadaikunnan, S.; Khaled, J.M.; Benelli, G. Biopolymer gelatin-coated zinc oxide nanoparticles showed high antibacterial, antibiofilm and anti-angiogenic activity. *J. Photochem. Photobiol. B Biol.* **2018**, *178*, 211–218. [CrossRef]
20. Sun, Z.; Qin, R.; Li, D.; Ji, K.; Wang, T.; Cui, Z.; Huang, Y. A novel bacterial type II l-asparaginase and evaluation of its enzymatic acrylamide reduction in French fries. *Int. J. Biol. Macromol.* **2016**, *92*, 232–239. [CrossRef]
21. Torkaman, R.; Darvishi, S.; Jokar, M.; Kharaziha, M.; Karbasi, M. Electrochemical and in vitro bioactivity of nanocomposite gelatin-forsterite coatings on AISI 316L stainless steel. *Prog. Org. Coat.* **2017**, *103*, 40–47. [CrossRef]
22. Cañaveral, S.; Morales, D.; Vargas, A.F. Synthesis and characterization of a 58S bioglass modified with manganese by a sol-gel route. *Mater. Lett.* **2019**, *255*, 126575. [CrossRef]
23. Khosravi, F.; Khorasani, S.N.; Khalili, S.; Neisiany, R.E.; Ghomi, E.R.; Ejeian, F.; Das, O.; Nasr-Esfahani, M.H. Development of a Highly Proliferated Bilayer Coating on 316L Stainless Steel Implants. *Polymers* **2020**, *12*, 1022. [CrossRef] [PubMed]
24. Macuvele, D.L.P.; Nones, J.; Matsinhe, J.V.; Lima, M.M.; Soares, C.; Fiori, M.A.; Riella, H.G. Advances in ultra high molecular weight polyethylene/hydroxyapatite composites for biomedical applications: A brief review. *Mater. Sci. Eng. C* **2017**, *76*, 1248–1262. [CrossRef] [PubMed]
25. Mesquita-Guimarães, J.; Ramos, L.; Detsch, R.; Henriques, B.; Fredel, M.; Silva, F.; Boccaccini, A.R. Evaluation of in vitro properties of 3D micro-macro porous zirconia scaffolds coated with 58S bioactive glass using MG-63 osteoblast-like cells. *J. Eur. Ceram. Soc.* **2019**, *39*, 2545–2558. [CrossRef]
26. Boodagh, P.; Johnson, R.; Maly, C.; Ding, Y.; Tan, W. Soft-sheath, stiff-core microfiber hydrogel for coating vascular implants. *Colloids Surf. B Biointerfaces* **2019**, *183*, 110395. [CrossRef]
27. Hanas, T.; Kumar, T.S.; Perumal, G.; Doble, M.; Ramakrishna, S. Electrospun PCL/HA coated friction stir processed AZ31/HA composites for degradable implant applications. *J. Mater. Process. Technol.* **2018**, *252*, 398–406.
28. Yang, G.; Chen, H.; Qin, H.; Feng, Y. Amination of activated carbon for enhancing phenol adsorption: Effect of nitrogen-containing functional groups. *Appl. Surf. Sci.* **2014**, *293*, 299–305. [CrossRef]
29. Ananth, K.P.; Nathanael, A.J.; Jose, S.P.; Oh, T.H.; Mangalaraj, D. A novel silica nanotube reinforced ionic incorporated hydroxyapatite composite coating on polypyrrole coated 316L SS for implant application. *Mater. Sci. Eng. C* **2016**, *59*, 1110–1124. [CrossRef]
30. de Souza, E.A.; Giz, M.J.; Camara, G.A.; Antolini, E.; Passos, R.R. Ethanol electro-oxidation on partially alloyed Pt-Sn-Rh/C catalysts. *Electrochim. Acta* **2014**, *147*, 483–489. [CrossRef]
31. Kumar, A.M.; Nagarajan, S.; Ramakrishna, S.; Sudhagar, P.; Kang, Y.S.; Kim, H.; Gasem, Z.M.; Rajendran, N. Electrochemical and in vitro bioactivity of polypyrrole/ceramic nanocomposite coatings on 316L SS bio-implants. *Mater. Sci. Eng. C* **2014**, *43*, 76–85. [CrossRef] [PubMed]
32. Kumar, A.M.; Sudhagar, P.; Fujishima, A.; Gasem, Z.M. Hierarchical polymer nanocomposite coating material for 316L SS implants: Surface and electrochemical aspects of PPy/f-CNTs coatings. *Polymer* **2014**, *55*, 5417–5424. [CrossRef]

33. Kichi, M.K.; Torkaman, R.; Mohammadi, H.; Toutounchi, A.; Kharaziha, M.; Alihosseini, F. Electrochemical and in vitro bioactivity behavior of Poly (ε-caprolactone)(PCL)-Gelatin-Forsterite Nano Coating on Titanium for Biomedical Application. *Mater. Today Commun.* **2020**, *24*, 101326. [CrossRef]
34. Matsuo, T. Trehalose protects corneal epithelial cells from death by drying. *Br. J. Ophthalmol.* **2001**, *85*, 610–612. [CrossRef] [PubMed]
35. Won, Y.-W.; Patel, A.N.; Bull, D.A. Cell surface engineering to enhance mesenchymal stem cell migration toward an SDF-1 gradient. *Biomaterials* **2014**, *35*, 5627–5635. [CrossRef] [PubMed]
36. Iso, B.; Standard, B. Biological evaluation of medical devices. *Part* **2009**, *1*, 10993.
37. Yang, Y.; Zheng, K.; Liang, R.; Mainka, A.; Taccardi, N.; Roether, J.A.; Detsch, R.; Goldmann, W.H.; Virtanen, S.; Boccaccini, A.R. Cu-releasing bioactive glass/polycaprolactone coating on Mg with antibacterial and anticorrosive properties for bone tissue engineering. *Biomed. Mater.* **2017**, *13*, 015001. [CrossRef]
38. Gorustovich, A.A.; Roether, J.A.; Boccaccini, A.R. Effect of bioactive glasses on angiogenesis: A review of in vitro and in vivo evidences. *Tissue Eng. Part B Rev.* **2010**, *16*, 199–207. [CrossRef]
39. Rahaman, M.N.; Day, D.E.; Bal, B.S.; Fu, Q.; Jung, S.B.; Bonewald, L.F.; Tomsia, A.P. Bioactive glass in tissue engineering. *Acta Biomater.* **2011**, *7*, 2355–2373. [CrossRef]
40. Sterling, D.L.; Thornton, J.D.; Swafford, A.; Gottlieb, S.; Bishop, S.; Stanley, A.; Downey, J.M. Hyperbaric oxygen limits infarct size in ischemic rabbit myocardium in vivo. *Circulation* **1993**, *88*, 1931–1936. [CrossRef]
41. Mahmoudi, M.; Raeissi, K.; Karimzadeh, F.; Golozar, M. A study on corrosion behavior of graphene oxide coating produced on stainless steel by electrophoretic deposition. *Surf. Coat. Technol.* **2019**, *372*, 327–342. [CrossRef]
42. Deligianni, D.D.; Katsala, N.D.; Koutsoukos, P.G.; Missirlis, Y.F. Effect of surface roughness of hydroxyapatite on human bone marrow cell adhesion, proliferation, differentiation and detachment strength. *Biomaterials* **2000**, *22*, 87–96. [CrossRef]
43. Lu, A.; Gao, Y.; Jin, T.; Luo, X.; Zeng, Q.; Shang, Z. Effects of surface roughness and texture on the bacterial adhesion on the bearing surface of bio-ceramic joint implants: An in vitro study. *Ceram. Int.* **2000**, *46*, 6550–6559. [CrossRef]
44. Coan, T.; Barroso, G.; Machado, R.; de Souza, F.; Spinelli, A.; Motz, G. A novel organic-inorganic PMMA/polysilazane hybrid polymer for corrosion protection. *Prog. Org. Coat.* **2015**, *89*, 220–230. [CrossRef]
45. Tan, O.; Cimen, O.; Yolcu, P.; ÇİÇEK, B. Development and characterisation of solvent-borne thermally cured cross-linked TiO2 reinforced Polyceramic coatings for long service-life on industrial metal substrates. *La Metall. Ital.* **2020**, *6*, 6–20.
46. Tamjid, E.; Bagheri, R.; Vossoughi, M.; Simchi, A. Effect of particle size on the in vitro bioactivity, hydrophilicity and mechanical properties of bioactive glass-reinforced polycaprolactone composites. *Mater. Sci. Eng. C* **2011**, *31*, 1526–1533. [CrossRef]
47. Tabesh, E.; Kharaziha, M.; Mahmoudi, M.; Shahnam, E.; Rozbahani, M. Biological and corrosion evaluation of Laponite®: Poly (caprolactone) nanocomposite coating for biomedical applications. *Colloids Surf. A Physicochem. Eng. Asp.* **2019**, *583*, 123945. [CrossRef]
48. Tabesh, E.; Salimijazi, H.; Kharaziha, M.; Mahmoudi, M.; Hejazi, M. Development of an in-situ chitosan-copper nanoparticle coating by electrophoretic deposition. *Surf. Coat. Technol.* **2019**, *364*, 239–247. [CrossRef]
49. Ataei, S.; Khorasani, S.N.; Torkaman, R.; Neisiany, R.E.; Koochaki, M.S. Self-healing performance of an epoxy coating containing microencapsulated alkyd resin based on coconut oil. *Prog. Org. Coat.* **2018**, *120*, 160–166. [CrossRef]
50. Li, S.; Ren, G.; Hoque, M.N.F.; Dong, Z.; Warzywoda, J.; Fan, Z. Carbonized cellulose paper as an effective interlayer in lithium-sulfur batteries. *Appl. Surf. Sci.* **2017**, *396*, 637–643. [CrossRef]
51. Wang, L.; Wei, Z.-L.; Chen, Z.-Z.; Liu, C.; Dong, W.-K.; Ding, Y.-J. A chemical probe capable for fluorescent and colorimetric detection to Cu2+ and CN− based on coordination and nucleophilic addition mechanism. *Microchem. J.* **2020**, *155*, 104801. [CrossRef]
52. Barrère, F.; van Blitterswijk, C.A.; de Groot, K. Bone regeneration: Molecular and cellular interactions with calcium phosphate ceramics. *Int. J. Nanomed.* **2006**, *1*, 317.
53. Dziadek, M.; Zagrajczuk, B.; Menaszek, E.; Cholewa-Kowalska, K. A new insight into in vitro behaviour of poly (ε-caprolactone)/bioactive glass composites in biologically related fluids. *J. Mater. Sci.* **2018**, *53*, 3939–3958. [CrossRef]

54. Islam, M.T.; Felfel, R.M.; Neel, E.A.A.; Grant, D.M.; Ahmed, I.; Hossain, K.M.Z. Bioactive calcium phosphate–based glasses and ceramics and their biomedical applications: A review. *J. Tissue Eng.* **2017**, *8*, 2041731417719170. [CrossRef] [PubMed]
55. Coletti, C.; Jaroszeski, M.J.; Hoff, A.; Saddow, S.E. SiC In Vitro Biocompatibility: Epidermal and Connective Tissue Cells. In *Silicon Carbide Biotechnology: A Biocompatible Semiconductor for Advanced Biomedical Devices and Applications*; Elsevier: Amsterdam, The Netherlands, 2011; pp. 119–151.
56. Makino, H.; Emi, H.; Yamaguchi, A.; Iritani, E.; Namiki, N.; Myojo, T.; Yamamoto, K. Environmental and safety issues with nanoparticles. In *Nanoparticle Technology Handbook*; Elsevier: Amsterdam, The Netherlands, 2008; pp. 385–417.
57. Mishra, D.; Iyyanki, T.; Hubenak, J.; Zhang, Q.; Mathur, A.B. Silk fibroin nanoparticles and cancer therapy. In *Nanotechnology in Cancer*; Elsevier: Amsterdam, The Netherlands, 2017; pp. 19–44.
58. Cadena-Herrera, D.; Lara, J.E.E.-D.; Ramírez-Ibañez, N.D.; López-Morales, C.A.; Pérez, N.O.; Flores-Ortiz, L.F.; Medina-Rivero, E. Validation of three viable-cell counting methods: Manual, semi-automated, and automated. *Biotechnol. Rep.* **2015**, *7*, 9–16. [CrossRef]
59. Baserga, C.; Massarelli, O.; Bolzoni, A.R.; Rossi, D.S.; Beltramini, G.A.; Baj, A.; Giannì, A.B. Fibula free flap pedicle ossification: Experience of two centres and a review of the literature. *J. Cranio Maxillofac. Surg.* **2018**, *46*, 1674–1678. [CrossRef]
60. Bemenderfer, T.B.; Davis, W.H.; Anderson, R.B.; Wing, K.; Escudero, M.I.; Waly, F.; Penner, M. Heterotopic ossification in total ankle arthroplasty: Case series and systematic review. *J. Foot Ankle Surg.* **2020**, *59*, 716–721. [CrossRef]